Range Extension Control System for Electric Vehicles during Acceleration and Deceleration Based on Front and Rear Driving-Braking Force Distribution Considering Slip Ratio and Motor Loss

Shingo Harada and Hiroshi Fujimoto
The University of Tokyo
5-1-5, Kashiwanoha, Kashiwa, Chiba, 277-8561 Japan
Phone: +81-4-7136-3881
Fax: +81-4-7136-3881
Email: harada@hflab.k.u-tokyo.ac.jp, fujimoto@k.u-tokyo.ac.jp

***Abstract*— Electric vehicles (EVs) have become a world-widely recognized solution for future green transportation. However, the mileage per charge of EVs is short compared with that of internal combustion engine vehicles. Considering slip ratio, copper loss and iron loss, the authors propose a model-based range extension control system for acceleration and deceleration mode. Total driving-braking force is distributed based on vehicle acceleration and velocity. The effectiveness of the proposed method is verified by simulations and experiments.**

I. Introduction

Considering current environmental and energy problems, electric vehicles (EVs) have been proposed as an alternative solution to internal combustion engine vehicles (ICEVs). In addition, EVs have the remarkable advantages compared with ICEVs [1].

- Response of driving-braking force by motor is much faster than that of engines (100 times).
- In-wheel motors enable independent control and drive of each wheel.
- Motor torque is measured precisely from motor current.

Research of traction control [2], [3] and stability control [4] utilizing the above advantages were actively conducted.

One of the reasons that prevents EVs from spreading is that mileage pet charge of EVs is shorter than that of conventional ICEVs. In order to solve this problem, research on efficiency improvement of motors [5] and regenerative torque control [6] were carried out. From the view point of motor efficiency control, research of torque and angular velocity pattern that maximize efficiency during acceleration and deceleration [7] was carried out. Utilizing independent characteristic of traction motors, a torque distribution method was studied to decrease EV's energy consumption [8].

On the other hand, the authors' research group proposed range extension control systems (RECSs) [9]–[11]. These systems do not involve changes of vehicle structure such as additional clutch [8] and motor type. RECS extends cruising range by motion control of vehicle. However, conventional RECS during straight driving involve pre-calculation of optimal torque distribution ratio for every driving condition from efficiency map of front and rear motor [9] or time-consuming search control to detect torque distribution ratio that maximize total efficiency [10].

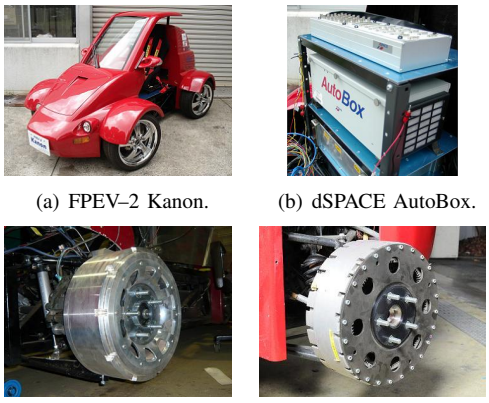

(a) FPEV–2 Kanon. (b) dSPACE AutoBox.

(c) Front Motor. (d) Rear Motor.

Fig. 1. Experimental Vehicle.

In this paper, a model-based RECS during straight driving is proposed. This method considers load transfer and motor loss and derives driving force distribution ratio that minimize inverter input power. Since this distribution ratio only depends on vehicle velocity and acceleration, it is unnecessary to perform pre-calculation and search control. Therefore, the proposed method is effective not only for constant speed but also for acceleration and deceleration. The effectiveness of the proposed method is verified by simulations and experiments.

II. Experimental Vehicle and Vehicle Model

A. Experimental Vehicle

In this research, an original electric vehicle "FPEV–2 Kanon", manufactured by the authors' research group, is used. This vehicle has four outer-rotor type in-wheel motors. Since these motors are direct drive type, the reaction force from road

TABLE I

VEHICLE SPECIFICATION.

Vehicle Mass M	854 kg
Wheelbase l	1.715 m
Distance from CG to front/rear axle l_f, l_r	l_f:1.013 m l_r:0.702 m
Gravity height h_g	0.51 m
Front Wheel Inertia J_{ω_f}	1.24 Nms^2
Rear Wheel Inertia J_{ω_r}	1.26 Nms^2
Wheel Radius r	0.302 m

TABLE II

SPECIFICATION OF IN–WHEEL MOTORS.

	Front	Rear
Manufacturer	TOYO DENKI SEIZO K.K.	
Type	Direct Drive System Outer Rotor Type	
Rated Torque	110 Nm	137 Nm
Maximum Torque	500 Nm	340 Nm
Rated Power	6.0 kW	4.3 kW
Maximum Power	20.0 kW	10.7 kW
Rated Speed	382 rpm	300 rpm
Maximum Speed	1113 rpm	1500 rpm

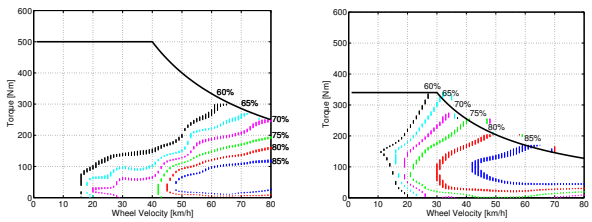

(a) Front Motor. (b) Rear Motor.

Fig. 2. Efficiency Maps of Front and Rear Motors.

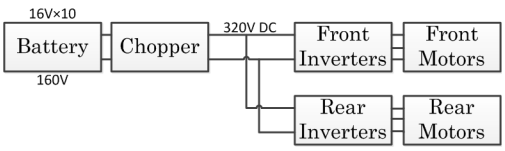

Fig. 3. Electric Power System of Vehicle.

is directly transferred to the motor without backlash influence of the reduction gear.

Fig. 1 shows the experimental vehicle. The dSPACE AutoBox (DS1103) is used for real-time data acquisition and control. Table I and Table II show the specification of vehicle and in-wheel motors. Fig. 2 expresses efficiency map of the front/rear in-wheel motors [9]. Since front/rear motors installed in the vehicle are different, efficiency maps of those are different. Therefore, extending cruising range by exploiting the difference of the efficiency is possible.

Fig. 3 illustrates power system of the vehicle. Lithium-ion battery is used as power source. The voltage of the main battery is 160 V (ten battery modules are connected in series). The voltage is boosted to 320 V by a chopper. In this paper, the chopper loss is neglected.

B. Vehicle Model

In this section, a four wheel driven vehicle model is described. The equation of wheel rotation is expressed as (1).

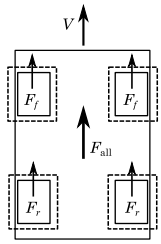

Fig. 4. Vehicle Model.

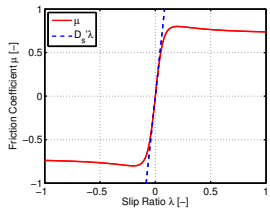

Fig. 5. Example of μ-λ Curve.

In case of straight driving, driving-braking forces of right and left wheels are equal. From Fig. 4, the equations of vehicle dynamics are expressed as

$$J_{\omega_j}\dot{\omega}_j = T_j - rF_j, \tag{1}$$

$$M\dot{V} = F_{\mathrm{all}} - F_{\mathrm{DR}} = 2(F_f + F_r) - F_{\mathrm{DR}}, \tag{2}$$

$$F_{\mathrm{all}} = 2(F_f + F_r), \tag{3}$$

where ω_j[rad/s] is the wheel angular velocity, V[m/s] is the vehicle speed, T_j[Nm] is the motor torque, F_{all}[N] is the total driving-braking force, F_j[N] is the each driving-braking force, M[kg] is the vehicle mass, r[m] is the wheel radius, $J_{\omega_j}[\mathrm{Nms}^2]$ is the wheel inertia, and F_{DR}[N] is the driving resistance. The subscript j represents f or r, which stands for front or rear wheel.

Next, the slip ratio λ_j is defined as

$$\lambda_j = \frac{V_{\omega_j} - V}{\max(V_{\omega_j}, V, \epsilon)}, \tag{4}$$

where $V_{\omega_j} = r\omega_j$ is the wheel speed and ϵ is a small constant to avoid zero division. It is known the slip ratio λ has the relationship with the coefficient of friction μ as shown Fig. 5 [13]. In region $|\lambda| \ll 1$, μ is nearly proportional to λ. Let D_s' be the slope of the curve, driving force of each tire is expressed as

$$F_j = \mu_j N_j \approx D_s' N_j \lambda_j. \tag{5}$$

The normal forces of each wheel during longitudinal acceleration process are calculated as

$$N_f(a_x) = \frac{1}{2}\left(\frac{l_r}{l}Mg - \frac{h_g}{l}Ma_x\right), \tag{6}$$

$$N_r(a_x) = \frac{1}{2}\left(\frac{l_f}{l}Mg + \frac{h_g}{l}Ma_x\right), \tag{7}$$

where N_f and N_r are the front and rear normal forces, respectively, $a_x[\mathrm{m/s}^2]$ is the longitudinal acceleration, l_f and l_r[m] are the distance from center of gravity to front and rear axle, h_g[m] is the center-of-gravity height. Acceleration direction is defined as positive.

III. DRIVING-BRAKING FORCE DISTRIBUTION CONTROL

A. Driving-Braking force distribution model

During straight driving, required total driving-braking force can be distributed to each wheel. Since the motors of the EV assumed in this research can be independently controlled, a degree of freedom of the driving-braking force distribution

exists. Introducing front and rear driving-braking force distribution ratio k, driving-braking forces can be formulated based on the total driving-braking force $F_{\rm all}$ using the distribution ratio k, as follows [10]:

$$F_f = \frac{1}{2}(1-k)F_{\rm all}, \quad (8)$$

$$F_r = \frac{1}{2}kF_{\rm all}. \quad (9)$$

Distribution ratio k varies between 0 and 1. $k=0$ means the vehicle is a front driven system, and $k=1$ means rear driven only.

B. Modeling of inverter input power

In this subsection, considering the slip ratio and motor loss, distribution ratio that minimizes the inverter input power is derived. Neglecting the inverter loss and mechanical loss of the motor, inverter input power $P_{\rm in}$ is expressed as

$$P_{\rm in} = P_{\rm out} + P_c + P_i, \quad (10)$$

where $P_{\rm out}$[W] is the sum of mechanical output of each motor, P_c[W] is the sum of copper loss of each motor, P_i[W] is the sum of iron loss of each motor. $P_{\rm out}$ is given by

$$P_{\rm out} = 2(\omega_f T_f + \omega_r T_r). \quad (11)$$

In the modeling of copper loss P_c, iron loss is neglected for simplification. Let us suppose that magnet torque is much bigger than reluctance torque, and q-axis current is much bigger than d-axis current, the sum of copper loss of the permanent magnetic motors P_c is expressed as

$$P_c = 2(R_f i_{qf}^2 + R_r i_{qr}^2), \quad (12)$$

where R_f and R_r[Ω] are the armature winding resistance of front and rear motor, respectively, i_{qf} and i_{qr}[A] are q-axis and d-axis current of front and rear motor, respectively. Then, following relationship between q axis current and torque is obtained,

$$i_{qj} = \frac{T_j}{K_{tj}} = \frac{T_j}{P_{nj}\Psi_j}, \quad (13)$$

where K_{tj}[Nm/A] is the torque coefficient of the motor, P_{nj} is the number of pole pairs, and Ψ_j[Wb] is the interlinkage magnetic flux. Therefore, copper loss P_c is given by

$$P_c = 2\left(\frac{R_f T_f^2}{K_{tf}^2} + \frac{R_r T_r^2}{K_{tr}^2}\right). \quad (14)$$

In this paper, equivalent circuit model [14] is used to examine iron loss. Fig. 6 shows d and q axis equivalent circuits of permanent magnetic motor. From the circuits, the iron loss of each motor P_{ij} is expressed as

$$P_{ij} = \frac{\omega_{ej}^2}{R_{cj}}\left\{(L_{dj}i_{odj} + \Psi_j)^2 + (L_{qj}i_{oqj})^2\right\}, \quad (15)$$

where ω_{ej}[rad/s] is the electrical angular velocity of each motor, R_{cj}[Ω] is the equivalent iron loss resistance, L_{dj}[H] is d-axis inductance, L_{qj}[H] is q-axis inductance, i_{odj} and

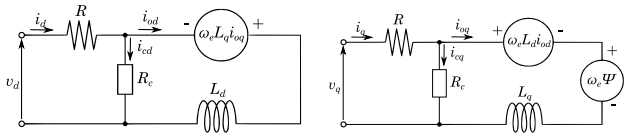

(a) d-axis. (b) q-axis.

Fig. 6. Equivalent Circuit of PMSM.

i_{oqj}[A] are the difference between d and q-axis current i_{dj}, i_{qj} and d and q-axis components of iron loss current i_{cdj}, i_{cqj}, respectively [14]. In this paper, armature reaction of d-axis $\omega_e L_d i_{od}$ is neglected since it is much smaller than electromotive force of magnet. In addition, electrical angular velocity ω_{ej} is expressed by vehicle velocity V since slip ratio of each wheel is small. In this condition, iron loss is approximately calculated by

$$P_{ij} \approx \frac{V^2 P_{nj}^2}{r^2 R_{cj}}\left\{\left(\frac{L_{qj}}{K_{tj}}\right)^2 T_j^2 + \Psi_j^2\right\}. \quad (16)$$

Equivalent iron loss resistance R_{cj} is expressed as

$$\frac{1}{R_{cj}(\omega_{ej})} = \frac{1}{R_{c0j}} + \frac{1}{R'_{c1j}|\omega_{ej}|}. \quad (17)$$

In (17), the first and second terms of right-hand side mean eddy current loss and hysteresis loss [15].

From above equations, $P_{\rm in}$ is expressed as

$$\begin{aligned} P_{\rm in} &= P_{\rm out} + P_c + P_i \\ &= 2(\omega_f T_f + \omega_r T_r) + 2\left(\frac{R_f T_f^2}{K_{tf}^2} + \frac{R_r T_r^2}{K_{tr}^2}\right) \\ &\quad +2(P_{if}(V, T_f) + P_{ir}(V, T_r)). \end{aligned} \quad (18)$$

C. Optimal driving-braking force distribution ratio

In this subsection, optimal driving-braking force distribution ratio that minimizes input power of inverter is derived. The torque caused by inertial force of wheel can be neglected. Therefore, from (8) and (9), the front and rear motor torque T_f, T_r are expressed respectively as

$$T_f = rF_f = \frac{r}{2}(1-k)F_{\rm all}, \quad (19)$$

$$T_r = rF_r = \frac{r}{2}kF_{\rm all}. \quad (20)$$

If $|\lambda| \ll 1$, the slip ratio λ is approximated as $(V_{\omega_j} - V)/V$. Therefore, the wheel angular velocity of each wheel is expressed as

$$\omega_j = \frac{V}{r}(1+\lambda_j). \quad (21)$$

Substituting (16), (19), (20), and (21) to (18), $P_{\rm in}$ is obtained as

$$\begin{aligned} P_{\rm in}(k) &= VF_{\rm all}\left\{1+\lambda_f(k)+k(\lambda_r(k)-\lambda_f(k))\right\} \\ &+ \frac{r^2F_{\rm all}^2}{2}\left\{\frac{R_f(1-k)^2}{K_{tf}^2}+\frac{R_rk^2}{K_{tr}^2}\right\} \\ &+ \frac{V^2}{r^2}\left[\frac{P_{nf}^2}{R_{cf}(\omega_{ef})}\left\{\left(\frac{rL_{qf}(1-k)F_{\rm all}}{2K_{tf}}\right)^2+\Psi_f^2\right\}\right. \\ &+ \left.\frac{P_{nr}^2}{R_{cr}(\omega_{er})}\left\{\left(\frac{rL_{qr}kF_{\rm all}}{2K_{tr}}\right)^2+\Psi_r^2\right\}\right] \end{aligned} \tag{22}$$

where, from (5), (8) and (9), $\lambda_f(k), \lambda_r(k)$ is expressed respectively as

$$\lambda_f(k) = \frac{F_f}{D_s'N_f} = \frac{(1-k)F_{\rm all}}{2D_s'N_f}, \tag{23}$$

$$\lambda_r(k) = \frac{F_r}{D_s'N_f} = \frac{kF_{\rm all}}{2D_s'N_r}. \tag{24}$$

Since $P_{\rm in}(k)$ is a quadratic function of k, optimal distribution ratio $k_{\rm opt}$ satisfies $\partial P_{\rm in}/\partial k|_{k=k_{\rm opt}} = 0$. Therefore, $k_{\rm opt}$ is derived as a function of V and a_x as

$$k_{\rm opt}(V,a_x) = \frac{\frac{V}{D_s'N_f(a_x)}+\frac{r^2R_f}{K_{tf}^2}+\frac{V^2}{R_{cf}(\omega_{ef})}\left(\frac{L_{qf}}{\Psi_f}\right)^2}{\frac{V}{D_s'}\sum_{j=f,r}\frac{1}{N_j(a_x)}+r^2\sum_{j=f,r}\frac{R_j}{K_{tj}^2}+V^2\sum_{j=f,r}\frac{1}{R_{cj}(\omega_{ej})}\left(\frac{L_{qj}}{\Psi_j}\right)^2}. \tag{25}$$

IV. Simulation

A. Numerical Calculation

In this section, calculation of driving force distribution is conducted based on the values of Table I. Assume the vehicle runs on a high μ road, and driving stiffness D_s' is set to 12.

Equivalent iron loss resistance of front motor R_{cf} is determined as 18 Ω, and that of rear motor R_{c0r}, R_{c1r}' are determined as 10 Ω, 0.05 Ω, respectively, based on (17). Driving resistance $F_{\rm DR}$[N] is determined as

$$F_{\rm DR}(V) = \mu_0Mg + f_{\rm DR}(V), \tag{26}$$

where μ_0 is rolling friction coefficient, $f_{\rm DR}(V)$ is resistance including air resistance and viscous friction of wheels [12]. In this paper, considering low vehicle velocity, $f_{\rm DR}(V)$ is assumed to be proportional to V. μ_0 and the coefficient of $f_{\rm DR}(V)$ are 8.36×10^{-3} and 10.7 Ns/m, respectively. These values are obtained by experiments.

Fig. 7 shows a calculation result of $k_{\rm opt}$. $k_{\rm opt}$ increases with the increase of acceleration and decreases with the increase of deceleration. This is mainly because of the influence of variation of slip ratio caused by load transfer and copper loss. On the other hand, $k_{\rm opt}$ increases with the increase of vehicle velocity. The range of $k_{\rm opt}$ is from 0.2 to 0.45. This is because efficiency of the front motor is higher than that of the rear motor in wide area of efficiency map as shown in Fig. 2.

Fig. 8 shows calculation result of $P_{\rm in}$. Fig. 8(a) and Fig. 8(b) show results in case of $a_x = 1.0{\rm m/s^2}, V = 100$ km/h and $a_x = -3.0{\rm m/s^2}, V = 30$ km/h, respectively. In these figures, the values in case of $k = k_{\rm opt}$ are indicated by red dots. Fig. 8 indicates $P_{\rm in}$ is a convex function of k. Therefore, there is a k that minimizes $P_{\rm in}$. Although there are errors caused by approximations of torque, wheel angular velocity, copper loss and iron loss, the values in case of $k = k_{\rm opt}$ almost equal minimum values as can be observed in Fig. 8. Therefore, approximations assumed in this paper are appropriate.

B. Evaluation by pattern driving

In this section, to demonstrate the effectiveness of the proposed method, driving cycle-based evaluation is conducted. Fig. 9 shows the driving cycle, which is composed of acceleration, cruising and deceleration, and acceleration is 1.5 ${\rm m/s^2}$, maximum vehicle speed is 30 km/h and deceleration is -3.0 ${\rm m/s^2}$. To represent the relationship between road and tire, Magic Formula [13] is used.

Fig. 10 shows vehicle velocity control system to realize the vehicle velocity pattern in Fig. 9. This system is composed of a feedforward controller and a feedback controller. The input is vehicle velocity V, and these controllers generate total driving-braking force reference $F_{\rm all}^*$. And then, $F_{\rm all}^*$ is distributed to the front and rear driving-braking force reference F_j^* based on (8) and (9). Represented by the slip ratio, front and rear torque reference T_j^* is given as

$$T_j^* = rF_j^* + \frac{J_{\omega_j}a_x^*}{r}(1+\lambda_j^*), \tag{27}$$

where the second term of right hand side means compensation for inertia of the wheels. In this research, considering stability of vehicle velocity control system, reference of the acceleration a_x^* is used. λ_j^* is nominal slip ratio of front and rear wheels that is 0.05, 0 and -0.05 during acceleration, cruising and deceleration, respectively.

Vehicle velocity controller $C_{\rm PI}(s)$ is a PI controller, and it is designed by pole placement method. The plant of vehicle velocity controller is given by

$$\frac{V}{F_{\rm all}} = \frac{1}{Ms}, \tag{28}$$

In the simulation, the pole of vehicle velocity controller is set to -5 rad/s. This vehicle velocity control system corresponds to the driver model in Fig. 10.

Fig. 11 shows simulation results. Simulation is conducted in case of $k = 0, 0.5, k_{\rm opt}$. Fig. 11(a) shows vehicle velocity. The vehicle velocity of each case are equal, so driving condition of them are equal. Fig. 11(b) shows distribution ratio. Optimal distribution ratio $k_{\rm opt}$ increases during acceleration and decreases during deceleration. This result matches previous calculation. Fig. 11(c) and Fig. 11(d) show front and rear driving-braking forces, respectively. Total driving-braking force $F_{\rm all}$ is distributed based on k as shown by these figures.

Fig. 11(e)-(h) show energy consumption during acceleration, cruising, deceleration and overall driving cycle, respectively. These values are calculated by integration of $P_{\rm in}$. From

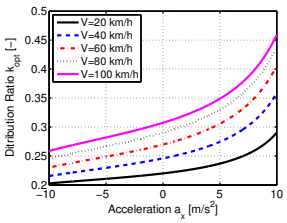

Fig. 7. Optimal Distribution Ratio.

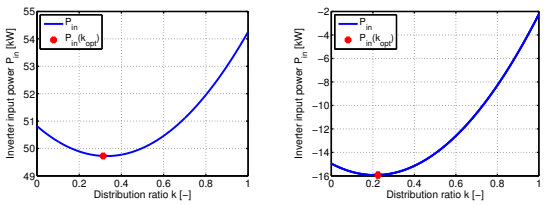

(a) a_x=1.0m/s^2, V=100 km/h. (b) a_x=-3.0m/s^2, V=30 km/h.

Fig. 8. Calculation Result of Inverter Input Power $P_{\rm in}$.

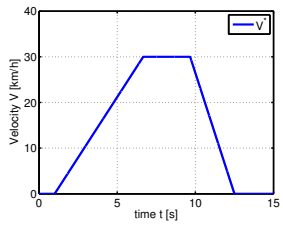

Fig. 9. Reference of Vehicle Speed.

Fig. 11(e) and Fig. 11(g), optimal distribution ratio $k_{\rm opt}$ minimizes energy consumption and maximizes regenerative energy. Therefore, $k_{\rm opt}$ minimizes total energy consumption. These results demonstrate effectiveness of the proposal method.

Table III shows cruising range per kWh. Cruising range is extended by 1.4 km per 1 kWh compared with the case of $k = 0.5$. Considering i-MiEV produced by MISTUBISHI MOTORS, which has a battery of 16 kWh, its cruising range can be extended by 22.4 km.

V. Experiment

Experiments are conducted under the same condition as simulation. In the experiment, the average of all the wheel velocities is treated as vehicle velocity. Inverter input power $P_{\rm in}$ is calculated as

$$P_{\rm in} \quad = \quad V_{\rm dc}(I_{{\rm dc}f} + I_{\rm dcr}), \tag{29}$$

where $V_{\rm dc}$[V] is the inverter input voltage, $I_{{\rm dc}f}$[A] is the front inverter input current, and $I_{\rm dcr}$[A] is the rear inverter input current. These values are measurable, and $P_{\rm in}$ includes inverter loss.

Fig. 12 shows experimental result. Since Fig. 12(a)-(d) are the same as simulation, behavior of the proposal algorithm is appropriate. From Fig. 12(c) and Fig. 12(d), it can be observed that front and rear driving-braking forces are vibrative. This is due to the influences of sensor noise and resolution of encoder.

Fig. 11(e)-(h) show energy consumption during acceleration, cruising, deceleration and overall driving cycle, respectively. In order to confirm repeatability of the experimental results, average values of 14 times experiments. In addition, standard deviation of each result is shown as error bars.

From Fig. 12(h), the case of $k_{\rm opt}$ achieves reduction of energy consumption compared with the cases when $k = 0$ and $k = 0.5$. Since experimental results include mechanical loss and inverter loss, energy consumption of experiment is bigger than that of simulation.

Table IV shows cruising range calculated by the same method as simulation. With the proposed method, cruising range per 1 kWh and 16 kWh are extended by 0.9 km and 14.2 km, respectively.

VI. Conclusion

This paper proposed an optimal front and rear driving-braking force distribution methodology which minimizes inverter input power. The effectiveness of the proposed model-based method was verified by simulations and experiments. In the experiments, cruising range per 1 kWh was extended by 0.9 km compared with the case of equal distribution.

The future works are to combine the proposed method with search method [10] and to achieve further efficiency improvement by using motor current control.

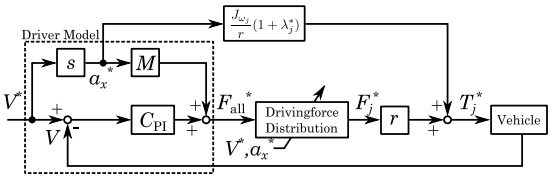

Fig. 10. Vehicle Speed Control System.

TABLE III

Cruising Range (simulation results).

k	0	$k_{\rm opt}$	0.5
1 kWh	5.93 km	6.60 km	5.21 km
16 kWh	94.90 km	105.6 km	83.31 km

TABLE IV

Cruising Range (experimental results).

k	0	$k_{\rm opt}$	0.5
1 kWh	4.33 km	5.19 km	4.26 km
16 kWh	69.35 km	83.05 km	68.11 km

Acknowledgement

This research was partly supported by Industrial Technology Research Grant Program from New Energy and Industrial Technology Development Organization(NEDO) of Japan (number 05A48701d), and by the Ministry of Education, Culture, Sports, Science and Technology grant (number 22246057).

References

[1] Y. Hori: "Future Vehicle Driven by Electricity and Control–Research on Four–Wheel–Motored:"UOT Electric March II"", IEEE Trans. IE, Vol. 51, No. 5, pp. 954–962 (2004)

[2] R. Shirato, T. Akiba, T. Fujita and S. Shimodaira: "A Study of Novel Traction Control Method for Electric Propulsuon Vehicle", Journal of the Society of Instrument and Control Engineers, Vol. 50, No. 3, pp. 195–200 (2011) (in Japanese)

[3] K. Maeda, H. Fujimoto, Y. Hori: "Four–wheel Driving–force Distribution Method Based on Driving Stiffness and Slip Ratio Estimation for Electric Vehicle with In–wheel Motors", the 8th IEEE Vehicle Power and Propulsion Conference, pp. 1286–1291 (2012)

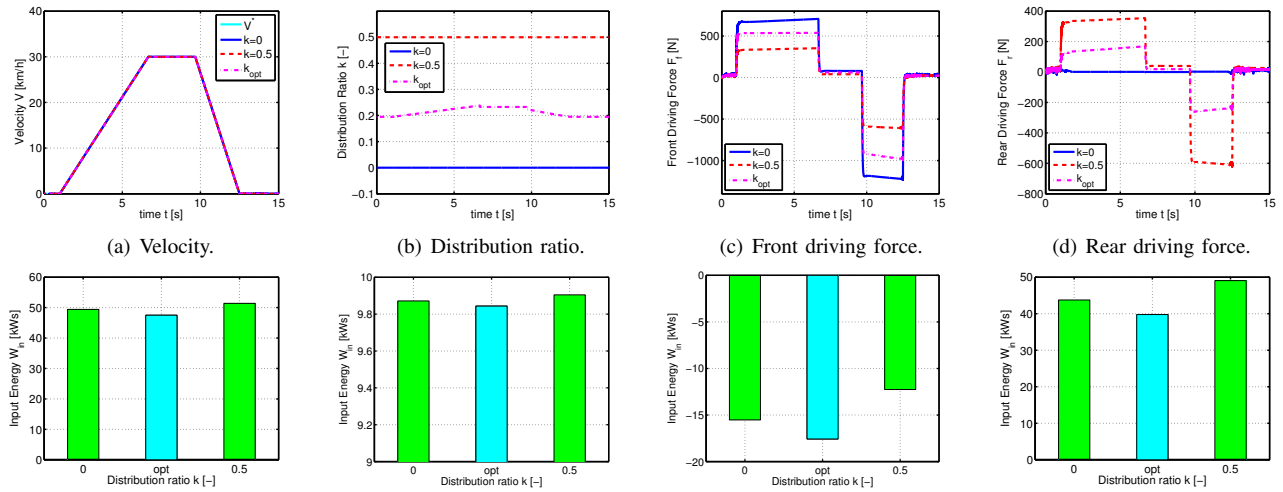

(a) Velocity. (b) Distribution ratio. (c) Front driving force. (d) Rear driving force.

(e) Inverter input energy (Acceleration). (f) Inverter input energy(Cruising). (g) Inverter input energy (Deceleration). (h) Inverter input energy(Total).

Fig. 11. Simulation Results.

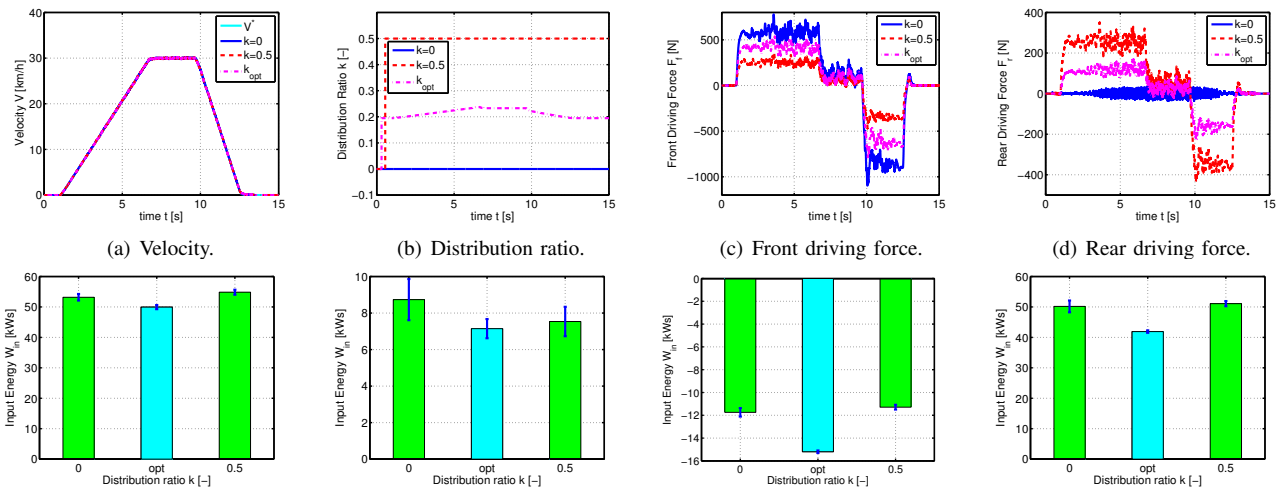

(a) Velocity. (b) Distribution ratio. (c) Front driving force. (d) Rear driving force.

(e) Inverter input energy (Acceleration). (f) Inverter input energy(Cruising). (g) Inverter input energy (Deceleration). (h) Inverter input energy(Total).

Fig. 12. Experimental Results.

[4] N. Ando, H. Fujimoto:"Yaw–rate control for electric vehicle with active front/rear steering and driving/braking force distribution of rear wheels", in Proc. the 11th IEEE International Workshop on Advanced Motion Control, pp. 726–731 (2010)

[5] H. Toda, Y. Oda, M. Kohno, M. Ishida and Y. Zaizen: "A New High Flux Density Non–Oriented Electrical Steel Sheet and its Motor Performance", IEEE Trans. MAGNETICS, Vol. 48, No. 11, pp. 3060–3063 (2012)

[6] B.R. Liang, W.S. Lin: "Optimal Regenerative Torque Control to Maximize Energy Recapture of Electric Vehicles", in Proc. World Automation Congress, (2010)

[7] K. Inoue, K. Kotera and T. Kato: "Optimal Motion Trajectories Minimizing Loss of Induction Motor under Amplitude Limits", in Proc. Energy Conversion Congress and Exposition, IEEE (2012)

[8] X. Yuan, J. Wang: "Torque Distribution Strategy for a Front– and Rear–Wheel–Driven Electric Vehicle", IEEE Trans. Veh. Technol., Vol. 61, No. 8, pp. 3365–3374 (2012)

[9] T. Suzuki, H. Fujimoto: "Proposal of Range Extension Control System by Drive and Regeneration Distribution Based on Efficiency Characteristic of Motors for Electric Vehicle", in Proc. IEE of Japan Technical Meeting Record, IIC–10–019, pp. 23–28 (2010) (in Japanese)

[10] H. Fujimoto, S. Egami, J. Saito, and K. Handa: "Range Extension Control System for Electric Vehicle Based on Searching Algorithm of Optimal Front and Rear Driving Force Distribution", in Proc. the 11th IEEE International Workshop on Advanced Motion Control (2012)

[11] H. Sumiya, H. Fujimoto: "Distribution Method of Front/Rear Wheel Side–Slip Angles and Left/Right Motor Torques for Range Extension Control System of Electric Vehicle on Curving Road", in Proc. 1st International Electric Vehicle Technology Conference (2011)

[12] S. Mori et al.: "Running Resistance of Rolling Stock", Journal of the J.S.M.E., Vol. 67, No. 543, pp. 620–630 (1964) (in Japanese)

[13] H.B. Pacejka and E. Bakker: "The Magic Formula Tyre Model", Vehicle System Dynamics: International Journal of Vehicle Mechanics and Mobility, Vol. 21, No. 1, pp. 1–18 (1992)

[14] S. Morimoto, Y. Tong, Y. Takeda, and T. Hirasa: "Loss Minimization Control of Permanent Magnet Synchronous Motor Drives", IEEE Trans. IE, Vol. 41, No. 5, pp. 511–517 (1994)

[15] S. Shinnaka: "Proposition of New Mathematical Models with Core Loss Factor for Controlling AC Motors", in Proc. of the 24–th Annual Conference of the IEEE Industrial Electronics Society, pp. 297–302 (1998)